ACS APPLIED MATERIALS & INTERFACES

Research Article

www.acsami.org

Titania Nanocoating on $MnCO_3$ Microspheres via Liquid-Phase Deposition for Fabrication of Template-Assisted Core–Shell- and Hollow-Structured Composites

Hack-Keun Lee,[†] Daisuke Sakemi,[†] Roman Selyanchyn,[†] Cheal-Gyu Lee,[‡] and Seung-Woo Lee*,[†]

[†]Graduate School of Environmental Engineering, The University of Kitakyushu, Kitakyushu 808-0135, Japan

[‡]Department of Environmental Engineering, Chongju University, Chongju 360-764, Korea

Supporting Information

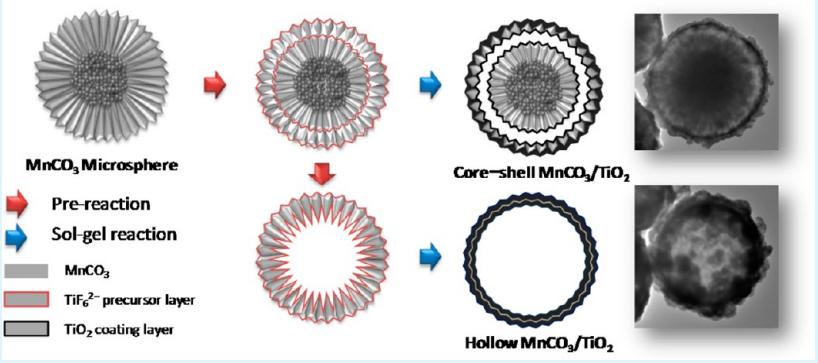

ABSTRACT: A novel class of core–shell- and hollow-structured $MnCO_3/TiO_2$ composites was synthesized by titania nanocoating on $MnCO_3$ microspheres via two-step liquid-phase deposition at room temperature. Morphological change from core–shell to hollow microparticles was possible in the prepared samples by controlling prereaction time of $MnCO_3$ and $[NH_4]_2TiF_6$. Upon the prereaction process, the core of the core–shell $MnCO_3/TiO_2$ became highly porous, and a honeycomb-like surface that resembled the orientation of self-assembled $MnCO_3$ nanocrystals was developed. The $MnCO_3$ core was completely removed after 6 h prereaction. Calcination at 600 °C resulted in the transformation of both core–shell- and hollow-structured composites to Mn_2O_3/TiO_2 anatase microspheres that retained their original morphologies. X-ray diffraction, field-emission scanning electron microscopy, Fourier transform infrared spectroscopy, transmission electron microscopy, and electron probe microanalysis were employed for microsphere characterization. As the first trial for application of the synthesized materials, solid-extraction of organics from aqueous media was examined using methylene blue (MB). Both types of Mn_2O_3/TiO_2 composites showed very fast adsorption of MB with high extraction values of 5.2 and 6.4 μmol g^{-1} for the core–shell and hollow structures, respectively. Current work provides a new approach for facile fabrication of titania–metal oxide nanocomposites with unique morphological features and promising application possibilities.

KEYWORDS: *manganese carbonate microspheres, liquid phase deposition, sol–gel reaction, titania nanocomposite, core–shell and hollow structures, organic pollutant extraction*

1. INTRODUCTION

TiO_2 materials have attracted considerable attention because of their unique features, such as strong oxidization ability, low environmental load, nontoxicity, and long-term photocatalytic activity. Recent research interests lie in their morphological control. So far, various nanostructures, such as wires,[1] tubes,[2] and films,[3,4] have been demonstrated. Among them, TiO_2 hollow structures have attracted special attention because of their high specific surface area, low density, and better permeability, and possess high potential for use as catalysts,[5] sensors,[6] and drug delivery carriers.[7]

In general, hollow-structured materials can be prepared either by template-assisted or by template-free methods. Template-free methods usually involve one-pot synthesis based on nanoscale corrosion-based inside-out evacuation,[8] Ostwald ripening,[9] or the Kirkendall effect.[10] Template-assisted methods are advantageous in providing more controlled structures, because of the reproducibility and the ease of the process.[5] The classical process involves the use of structure-directing agents such as gas bubbles[11] or emulsion droplets and micelles,[12,13] referred to as "soft" templates, and polymer latex spheres,[14,15] monodispersed silica[16,17] or carbon sphere[18] referred to as "hard" templates. The prepared samples have shown core–shell structures that can also be used as novel

Received: April 5, 2013
Accepted: December 9, 2013
Published: December 9, 2013

functional material in various fields.[19] After decomposition of the templates by calcination or etching, specific hollow structures can be obtained. Layer-by-layer deposition on a template polymer has also been extensively used to prepare uniform TiO_2 microcapsules;[5,20] however, it is a time-consuming process because it involves multistep deposition.

In this study, we introduce a novel approach for titania coating on $MnCO_3$ microspheres via liquid phase deposition (LPD), developed by Deki et al.,[21−23] which is a well-known method for fabrication of TiO_2 thin films. Titanium−fluoro complex anions can be adsorbed on $MnCO_3$ microspheres due to their electrostatic interaction with Mn^{2+} ions on the surface. To the best of our knowledge, the proposed approach is the first trial that uses $MnCO_3$ for fabricating core−shell- or hollow-structured $MnCO_3/TiO_2$ composites.

Many reports on titanium dioxides have focused on composites formed with manganese oxides. For instance, TiO_2-supported manganese oxides prepared by wet-impregnation exhibit selective catalytic reduction of NO_x with ammonia.[24] Interestingly, the manganese oxide contained in MnO_x-TiO_2 composites contributes to not only catalytic oxidation of organic compounds[25] but also to photocatalytic degradation of organic contaminants in aqueous solutions.[26]

A convenient, low-energy synthesis of crystalline TiO_2 is desirable because of its low synthetic cost and wide application. LPD is composed by the following reactions.[27] The process starts by the ligand exchange equilibrium reaction between a titanium−fluoro complex ion and water (eq 1). The addition of H_3BO_3 as a scavenger shifts the equilibrium to the right by consumption of fluoride ions (eq 2).

$$[NH_4]_2TiF_6 + 2H_2O \rightarrow TiO_2 + 2NH_4F + 4HF \quad (1)$$

$$H_3BO_3 + 4HF \rightarrow BF_4^- + H_3O^+ + 2H_2O \quad (2)$$

Microparticles of metal carbonates have been widely used as templates for the fabrication of organic microcapsules of polyelectrolyte multilayers, because the former can be easily and completely removed by acid treatment.[28] Among them, $MnCO_3$ is used as a typical precursor of manganese oxides, which are of considerable importance due to their potential applications in catalysis,[29,30] magnetic materials,[31,32] rechargeable batteries,[33,34] and supercapacitors.[35−37] In particular, the morphological diversity of $MnCO_3$, which includes nanoparticles,[38] nanowires,[39] and uniform microstructures,[40] provides great potential for its use as a template in the preparation of various forms of composite materials.

2. EXPERIMENTAL SECTION

2.1. Materials. Manganese sulfate monohydrate ($MnSO_4 \cdot H_2O$, Sigma-Aldrich Co.), sodium hydrogen carbonate ($NaHCO_3$, Kanto Chemical Co., Inc.), ammonium hexafluorotitanate ($[NH_4]_2TiF_6$, Mitsuwa Pure Chemicals), and boric acid (H_3BO_3, Wako Pure Chemical Industries, Ltd.) were used without further purification. Deionized water (18.2 MΩ cm^{-1}) was obtained by reverse osmosis and subsequently subjected to ion exchange and filtration in a Milli-Q apparatus.

2.2. Preparation of $MnCO_3$ Microspheres. Monodispersed $MnCO_3$ microspheres were synthesized through an improvement of the precipitation method reported by Antipov et al.[41] In brief, a 0.14 M $NaHCO_3$ solution was added to a 0.014 M $MnSO_4$ in a mixture of water and ethanol (5%, v/v) under vigorous agitation. The obtained solution was stirred for 4 h at room temperature. The resultant precipitates were filtered, washed with pure water and ethanol, and dried at 60 °C.

2.3. Sol−Gel Reaction by LPD. 50 mg of $MnCO_3$ microspheres were added as prepared to 10 mL of 0.1 M $[NH_4]_2TiF_6$ in water and slowly stirred for various time intervals ranging from 2 to 6 h (prereaction). After that, 10 mL of 0.2 M H_3BO_3 in water was added to the initial $[NH_4]_2TiF_6$ solution and additionally reacted under stirring for 12 h. The resultant particles were filtered, washed several times with water and ethanol, and dried at room temperature. These concentrations of both reagents for LPD process were optimized in preliminary experiments and used throughout the study. The samples were calcined at 600 °C for 3 h in air with a ramp rate of 10 °C min^{-1} in an electric muffle furnace (DenKen KDF S90).

2.4. Characterization. As-prepared and calcined products were characterized by X-ray diffraction (XRD, Rigaku XRD-DSC-X II) and field emission scanning electron microscopy (Hitachi S-5200, Japan). Prior to SEM measurements, samples were vacuum-dried for 6 h to thoroughly remove solvent and water adsorbed in the sample. To avoid electrical charge-up by the electron beam, the samples were coated with a thin (ca. 5 nm) platinum film using a Hitachi E-1030 ion sputter (15 mA, 10 Pa). Transmission electron microscope (TEM) micrographs were obtained using a JEOL JEM-3010 operating at 200 kV. Fourier transform infrared (FT-IR) spectra before and after TiO_2 coating were recorded in the wavenumber range of 4000−450 cm^{-1}, with a resolution of 1 cm^{-1}. Using KBr pellets, the spectra were recorded with a PerkinElmer Spectrum 100 FT-IR spectrometer at room temperature. An electron probe microanalyzer (EPMA, JEOL JXA-8100) was used to study the elemental distribution of Ti, Mn, and O species in the samples after calcination. To investigate the proton consumption of $MnCO_3$ microspheres, pH measurements of two aqueous solutions of 0.1 M $[NH_4]_2TiF_6$ with and without $MnCO_3$ microspheres were performed using an ISFET pH meter (KS701, Shindengen).

2.5. Adsorption Test. An aqueous solution of methlylene blue (MB, 10 μM) was used to investigate the adsorption property of calcined Mn_2O_3/TiO_2 anatase composites, which were adjusted to be 1.5 g L^{-1} in the solution. After MB adsorption for 30 s, the particles were precipitated by brief centrifugation and the clear supernatants were subjected to UV−vis spectroscopy measurements (V-570, Jasco Japan). Brynauer-Emmett-Teller (BET) surface area, pore size, and porosity of as-prepared and calcined composite samples were measured on a nitrogen adsorption apparatus (BELLSORP mini-II, Bell Japan).

3. RESULTS AND DISCUSSION

3.1. Preparation of $MnCO_3$ Microspheres. $MnCO_3$ microspheres were prepared by the reaction of $MnSO_4$ and $NaHCO_3$ in the presence of ethanol.[28] Figure S1 in the Supporting Information shows XRD patterns of the samples in the presence and absence of ethanol. A majority of the peaks from these as-prepared samples corresponds to rhombohedral $MnCO_3$ (JCPDS No. 44−1472). Figure 1 shows SEM images of the as-prepared $MnCO_3$ microparticles; differences in the morphology due to the presence of ethanol during preparation can also be seen. The shape of the obtained microspheres is significantly changed by addition of ethanol; spherical particles with a diameter of ca. 2.5 μm are obtained in the presence of ethanol (Figure 1a) whereas cubic particles of ca. 2 μm in size are obtained in the absence of ethanol (Figure 1c). Specifically, the use of ethanol becomes an important factor affecting crystal growth of $MnCO_3$, as can be observed under high magnification.

In this study, ethanol was used to decrease the dielectric constant of the reaction system; thus, the solubility of the inorganic salts may be suppressed.[26,39] Supersaturation of the inorganic salts, which can be accelerated by the addition of ethanol, will drive fast nucleation and growth of the solid phase. As a result, the initial $MnCO_3$ nanocrystals in the aggregate are presumed to be disoriented. Afterward, they grow up in

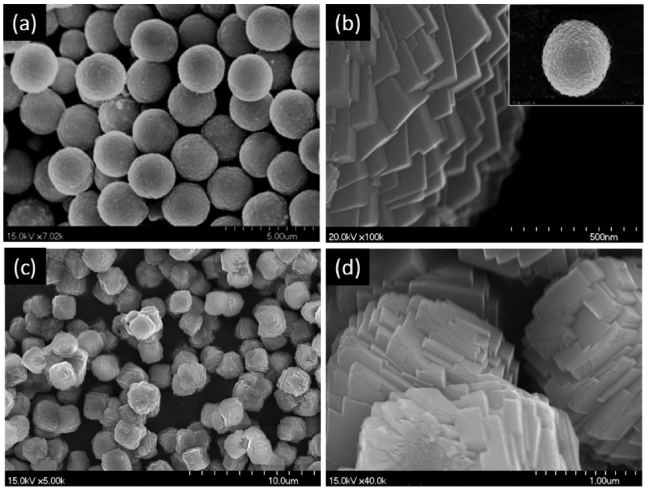

Figure 1. SEM images of $MnCO_3$ microspheres prepared in (a, b) presence and (c, d) absence of ethanol. Inset of b shows a whole image of the particle.

oriented form in different directions. Consequently, $MnCO_3$ flakes are fused at one end and branch out at the other end to form a multifaced crystal sphere.[42]

In addition, similar experiments were conducted using methanol and *n*-propanol, which have dielectric constants of 32.7 and 20.3 at 25 °C, respectively.[43] It is evident that uniform, spherical monodispersed $MnCO_3$ particles can be formed by the addition of solvents with low dielectric constants (see Figure S2 in the Supporting Information).

3.2. Sol–Gel Reaction via LPD. SEM measurement was conducted to follow the reaction between $MnCO_3$ and $[NH_4]_2TiF_6$ (prereaction). After 2 h prereaction, the sample showed a disordered core and etched spaces ca. 200 nm below the surface (Figure 2a). Interestingly, after a 6 h prereaction,

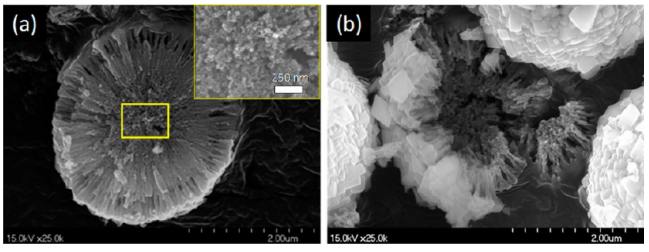

Figure 2. SEM images of $MnCO_3$ obtained with different prereaction times: (a) 2 and (b) 6 h. Inset of a shows a magnified image of the area enclosed by the yellow rectangle.

the core is completely removed, which was clearly observed in a broken microsphere (Figure 2b). Similar phenomena have been reported when acidic agents, such as HCl and EDTA, were used.[28] Different etching speeds in the core and shell may be caused by the different morphologies of $MnCO_3$ at these locations.

SEM images of the composites synthesized through LPD under different reaction conditions are given in Figures S3 and S4 in the Supporting Information. The concentration of $[NH_4]_2TiF_6$ and the prereaction time of $[NH_4]_2TiF_6$ and $MnCO_3$ are considered as important factors to determine the morphology of the composites, whereas the concentration of boric acid is not significant for such purpose. For further clear understanding of the composites, $MnCO_3/TiO_2$ composites synthesized through LPD for 12 h were subsequently examined by XRD, FT-IR, and TEM measurements.

Figure 3a shows XRD patterns of the samples synthesized by the sol–gel reaction described in the Experimental Section. The

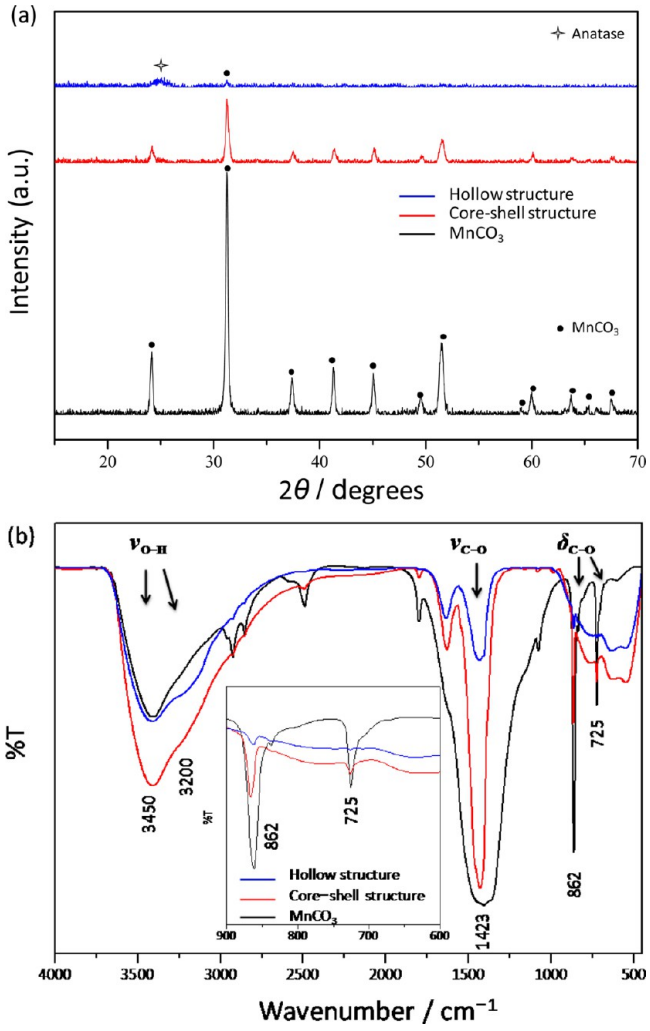

Figure 3. (a) XRD patterns and (b) FT-IR spectra of pure $MnCO_3$, core–shell $MnCO_3/TiO_2$ composite, and hollow $MnCO_3/TiO_2$ composite microspheres. Inset of b shows the respective spectra in the range 600–900 cm^{-1}.

XRD pattern of the core–shell $MnCO_3/TiO_2$ composite (prepared from the 2 h prereaction sample of Figure 2a) shows decreased $MnCO_3$ peaks, indicating suppression by the TiO_2 coating. In the case of the hollow $MnCO_3/TiO_2$ composite (prepared from the 6 h prereaction sample of Figure 2b), most of the $MnCO_3$ peaks disappeared, except for two trace peaks at around 25 and 31°, which can be attributed to the anatase TiO_2 (JCPDS No. 84–1285) and $MnCO_3$, respectively. This indicates that $MnCO_3$ was almost completely removed from the particle. From the XRD results, we conclude that $MnCO_3$ microspheres can be coated with TiO_2 through LPD, depending on the prereaction time with $[NH_4]_2TiF_6$.

FT-IR spectra of the products obtained by the sol–gel reaction and that of pure $MnCO_3$ are shown in Figure 3b. The spectrum of pure $MnCO_3$ shows the characteristic vibration bands of CO_3^{2-} at 1423, 862, and 725 cm^{-1}.[38] The broad peak centered at ca. 3450 cm^{-1} may be ascribed to the O–H

dx.doi.org/10.1021/am404052p | ACS Appl. Mater. Interfaces 2014, 6, 57–64

vibration of water adsorbed onto the $MnCO_3$ particle. After TiO_2 coating, the characteristic bands of CO_3^{2-} drastically decreased, especially in the 6 h prereaction sample. However, the TiO_2-coated samples reveal new vibration bands in the range 500−700 cm^{-1}, which originate from the Ti−O bond; these bands are usually observed in the as-prepared LPD samples. In addition, a new broad peak at ca. 3200 cm^{-1} is observed after TiO_2 coating. This peak is certainly attributable to the O−H vibration of Ti−OH moieties, which probably induce the enhanced intensity of the 3450 cm^{-1} band, because of the adsorption of water molecules.

Figure 4 shows SEM and TEM images of the core−shell particles prepared after TiO_2 coating via LPD. The SEM images

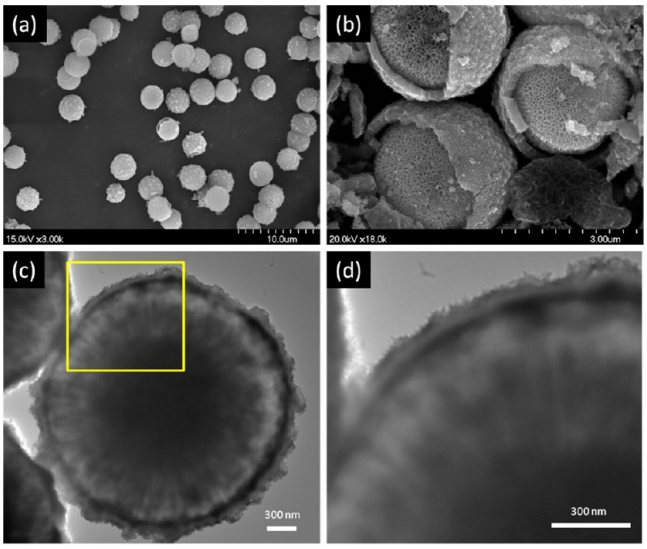

Figure 4. (a, b) SEM and (c) TEM images of core−shell $MnCO_3$/TiO_2 composite. (d) Magnified TEM image of the area enclosed by the yellow square inc.

(Figure 4a, b) demonstrate the formation of TiO_2-coated particles with a well-preserved spherical morphology. The obtained microspheres have an average diameter of ca. 3.0 μm, which is larger than that before TiO_2 coating. In particular, the particles exhibit smoother surfaces compared with the original $MnCO_3$ microspheres. To confirm the inner structure of the particle, the sample was mechanically crushed to break the TiO_2 shell. As clearly seen in Figure 4b, the particle has a hierarchical core with a diameter of ca. 2 μm. This unique particle structure having a shell composed of dense aggregates of TiO_2 nanoparticles can be seen more clearly in Figure 4c, d. The shell thickness is estimated to be 89 ± 14 nm. In addition, the empty (etched) space (see Figure 2a) between the shell and the core is also confirmed by the TEM images of the typical core−shell structure after TiO_2 coating.

Figure 5a shows an SEM image of the hollow $MnCO_3$/TiO_2 microspheres. It appears that a small hole is formed on the surface of the particles by the removal of the core. The cavity formed by the dissolved core can be clearly observed in the broken spheres (Figure 5b), which have a diameter of ca. 3.0 μm and an average shell thickness of 246 ± 12 nm. This hollow structure can be clearly seen in the TEM image in Figure 5c, indicating that the $MnCO_3$ core was completely removed from the particle. Interestingly, compared with that of the core−shell structure, the shell of the hollow sphere is thicker. The magnified SEM image (Figure 5d) reveals a thin line in the

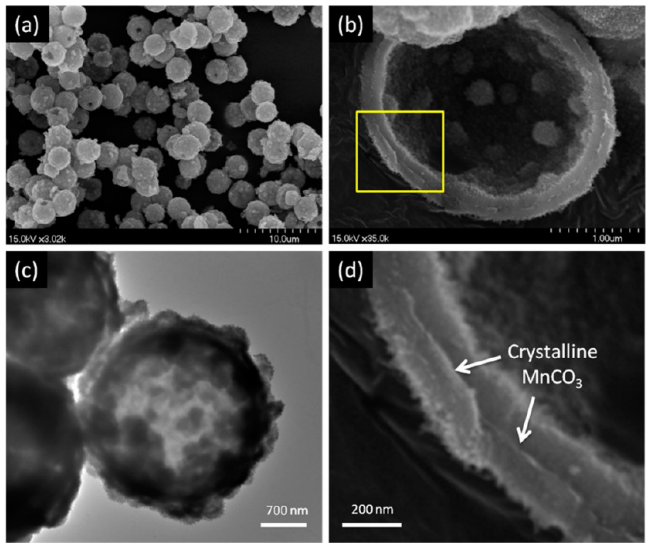

Figure 5. (a, b) SEM and (c) TEM images of hollow $MnCO_3$/TiO_2 composite. (d) Magnified SEM image of the area enclosed by the yellow square in b.

middle of the shell. Plausibly, this trace is the remaining crystalline $MnCO_3$ at the boundary of two TiO_2 coating layers: one from the surface, and the other from the interior.

3.3. Pathways for Composite Synthesis. The pathway leading to the core−shell and hollow $MnCO_3$/TiO_2 composite structures is shown in Scheme 1. Before prereaction $MnCO_3$ microspheres have two types of crystal structures inside the particle (Scheme 1a). When $[NH_4]_2TiF_6$ is added, TiF_6^{2-} will be adsorbed on the surface of the microspheres by forming an ion complex with Mn^{2+} ($MnCO_3$, K_{sp} = 2.24 × 10^{-11}). An additional reaction of $MnCO_3$ and HF (as a hydrolysis product of $[NH_4]_2TiF_6$) may proceed, as described in eq 3. This reaction is probably a key factor in the creation of the empty space and/or hollow interior. Differences in the pH of $[NH_4]_2TiF_6$ solutions with and without $MnCO_3$ are strong evidence of such reactions. The initial pH of the aqueous solutions of $[NH_4]_2TiF_6$ with and without $MnCO_3$ were 4.9 and 3.6, respectively, as shown in Figure S5 in the Supporting Information. This difference shows that the protons formed in the solution are immediately trapped into the $MnCO_3$ microspheres. Afterward, the pH of the solution gradually increased from 4.9 to 5.6 for 2-day reactions. Plausibly, this secondary, slow pH increase is related to the equilibrium reaction (eq 4) of free NH_4^+ and HCO_3^- ions, which are products of the reactions of eqs 1 and 3, respectively.

The protons trapped inside the particle make nanocavities near the surface by dissolving $MnCO_3$, as shown in Scheme 1b. Through this step, the protons can be diffused along the aligned $MnCO_3$ crystal lines into the interior, and the core, which is composed of $MnCO_3$ nanocrystals, begins to dissolve. A further, longer core evacuation process induces the formation of the hollow structure (Scheme 1c). In particular, the particles have a small hole on the surface of the TiO_2 shell, and this is probably formed by the release of carbon dioxide from the core (see Figure 5a).

$$2MnCO_3 + 4HF \rightarrow 2Mn^{2+} + 4F^- + 2H^+ + 2HCO_3^- \quad (3)$$

$$2NH_4^+ + 2HCO_3^- \rightleftarrows 2NH_3 + 2H_2O + 2CO_2(g) \quad (4)$$

dx.doi.org/10.1021/am404052p | ACS Appl. Mater. Interfaces 2014, 6, 57−64

Scheme 1. Schematic of the Synthesis of Core–Shell and Hollow $MnCO_3/TiO_2$ Composites: Cross-Sectional Illustrations of $MnCO_3$ Microsphere (a) before and (b, c) after Prereaction for 2 and 6 h with $[NH_4]_2TiF_6$, Respectively, and Their $MnCO_3/TiO_2$ Composites Showing (d) Core–Shell and (e) Hollow Structures after Sol–Gel Reaction for 12 h

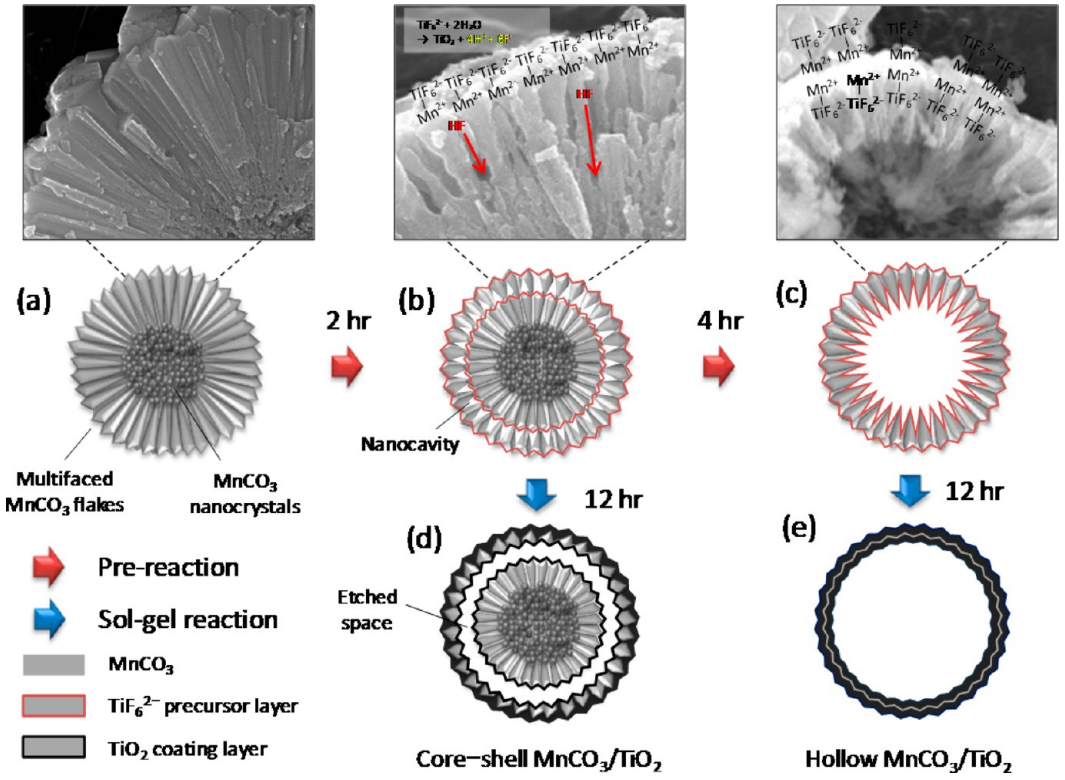

The adsorbed TiF_6^{2-} ions are transformed to TiO_2 by the sol–gel reaction with boric acid, which accelerates the reaction of eq 1 by trapping the F^- ions. In the case of the 2 h prereaction sample, the nanocavities near the surface become larger through the 12 h sol–gel reaction of LPD and the TiO_2-coated shell is separated from the core. Simultaneously, a TiO_2 coated honeycomb-like core is formed inside the particle, as shown in Scheme 1d. The honeycomb-like morphology of the core appears to be dependent on the crystal structure of the $MnCO_3$ flakes. The $MnCO_3$ core is almost etched after a prereaction longer than 6 h and an additional sol–gel reaction for 12 h. As a result, hollow-structured $MnCO_3/TiO_2$ is formed, as shown in Scheme 1e. In particular, the hollow sphere composite shows a specific shell structure that is composed of two TiO_2 coating layers around a boundary layer of crystalline $MnCO_3$ (see Figure 5d). The process for hollow structure formation can be explained as follows. First, TiO_2 coats the surface of spherical $MnCO_3$ flakes through the hydrolysis of complex ion TiF_6^{2-} moieties by water. Then, the diffused proton ions dissolve the $MnCO_3$ microspheres from the core.

To validate the feasibility of this method, a different type of $MnCO_3$, with a cubic structure of size ca. 2 μm, was also used as a template. Figure S6 in the Supporting Information shows results similar to those obtained with the spherical $MnCO_3$ template particles.

3.4. Calcination of $MnCO_3/TiO_2$ Composites. We also investigated the effect of calcination on the crystallinity and morphology of the core–shell and hollow $MnCO_3/TiO_2$ composites. The XRD patterns of the calcined core–shell and hollow $MnCO_3/TiO_2$ composites, shown in panels a and b in Figure 6, confirm that amorphous TiO_2 and $MnCO_3$ were

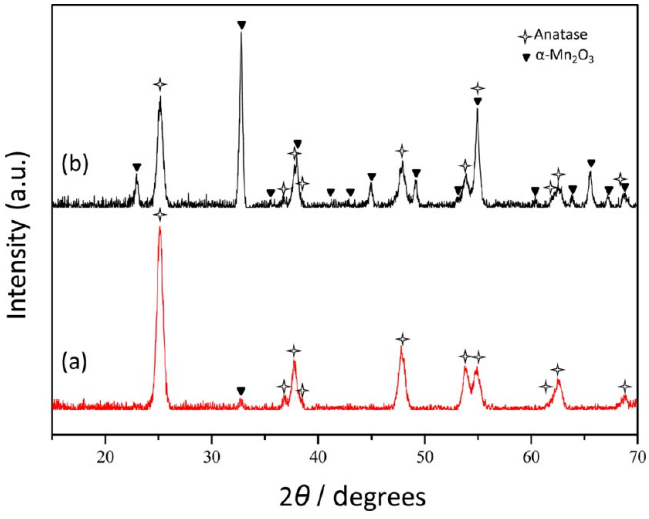

Figure 6. XRD patterns of calcined (a) core–shell and (b) hollow $MnCO_3/TiO_2$ composites.

transformed to crystalline anatase TiO_2 (JCPDS No. 84–1285) and α-Mn_2O_3 (JCPDS No. 89–4836), respectively. After thermal treatment at 600 °C for 3 h, the peaks assigned to α-Mn_2O_3 almost disappeared in the hollow $MnCO_3/TiO_2$ composite. Both the calcined products maintain the morphologies almost same as those before calcination, as shown in Figure 7; however, the surface of the TiO_2-coated $MnCO_3$ core shows rougher concaves after calcination (sea-urchin-like morphology), as shown in Figure S7 in the Supporting Information. In addition, the crystalline $MnCO_3$ boundary layer in the core–shell structure is not seen after calcination.

dx.doi.org/10.1021/am404052p | ACS Appl. Mater. Interfaces 2014, 6, 57–64

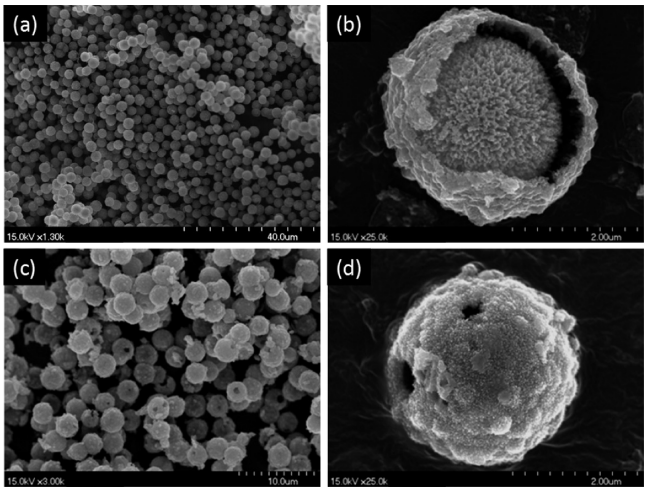

Figure 7. SEM images of Mn_2O_3/TiO_2 composites obtained after calcination at 600 °C for 3 h: (a, b) core−shell structure and (c, d) hollow structure.

Interestingly, the calcination led to a change in the color of the material from light brown to dark brown, as shown in Figure S8 in the Supporting Information; this is caused by the change in crystal structure from $MnCO_3$ to Mn_2O_3. The results of XRD and SEM demonstrate that the as-prepared microstructures became much stable by the heat-treatment.

In addition, EPMA analysis provided information about the chemical composition of the core−shell and hollow Mn_2O_3/TiO_2 composites; their wavelength-dispersive spectroscopy results are shown in Figure S9 in the Supporting Information. The characteristic atomic ratios for Ti, Mn, O, and other elements originating from the composites are shown in Table 1.

Table 1. Atomic Ratio of Elements in Mn_2O_3/TiO_2 Composites

	core−shell structure		hollow structure	
element	mass (%)	atom (%)	mass (%)	atom (%)
Ti	18.6	9.02	42.6	22.1
Mn	24.0	10.1	9.86	4.46
O	54.9	79.7	47.0	73.0
other	2.57	1.14	0.58	0.45
total	100	100	100	100

The core−shell Mn_2O_3/TiO_2 composite has a higher elemental ratio of Mn than the hollow Mn_2O_3/TiO_2 composite, which is in agreement with the result from the XRD analysis (see Figure 6). Conversely, the amount of Ti is relatively high in the case of the hollow Mn_2O_3/TiO_2 composite, and it increases from 9.02 to 22.1% when the composite structure is transformed from core−shell to hollow.

Figure 8 shows X-ray mapping images of Ti, Mn, and O by EPMA analysis. The two composite samples show inverse mapping images for Ti and Mn elements. Mn is more intensively observed in the core−shell Mn_2O_3/TiO_2 composite, as shown in Figure 8c. In contrast, the hollow Mn_2O_3/TiO_2 composite reveals a higher Ti content, as shown in Figure 8f.

3.5. Adsorption Properties. To screen application possibilities of the synthesized composites, first of all, their adsorption capability was examined using methlylene blue (MB). Figure 9 shows UV−vis absorption spectral changes of MB (10 μM in water) in the presence of the core−shell or hollow Mn_2O_3/TiO_2 composite (1.5 g L^{-1}). After addition of a certain volume of the MB solution to the respective composite, the mixture was immediately shaken for 30 s. After 30 s adsorption, the absorption spectrum of MB was drastically reduced, especially in the case of the hollow composite. The inset of Figure 9 shows a photograph showing colorimetric image of MB before and after adsorption test, evidencing the UV−vis results. A characteristic absorption peak of MB at 664.5 nm was chosen for comparing the adsorption capacity of the calcined samples, showing 77 and 95% absorbance decreases for the core−shell and hollow Mn_2O_3/TiO_2 composites, respectively. Consequently, the adsorbed density of MB is estimated to be 5.2 and 6.4 μmol g^{-1} for the core−shell and hollow Mn_2O_3/TiO_2 composites, respectively.

BET surface areas of the core−shell and hollow Mn_2O_3/TiO_2 composites were estimated to be 83.6 and 21.4 m^2 g^{-1}, respectively (see Figure S11 in the Supporting Information, 138.0 m^2 g^{-1} for the core−shell $MnCO_3/TiO_2$ composite before calcination). In spite of the smaller surface area of the hollow composite, it shows a higher binding capacity than the core−shell structure. This result indicates that the adsorption capability of the composites is probably dependent on their pore volume rather than their surface area or pore size, showing a good agreement with the UV−vis results. Interestingly, it was observed that MB was not efficiently adsorbed in the as-prepared $MnCO_3/TiO_2$ composites or calcined pure α-Mn_2O_3 microspheres, showing a smaller change less than 10% compared with the original spectrum of MB (data not shown). At the present stage, unfortunately, we do not have enough experimental data to explain the detailed mechanism of such adsorption behavior. Other parameters that assist the adsorption should be considered. Also, other investigations of the prepared composites, in particular for their photocatalytic properties, are currently in progress.

4. CONCLUSIONS

We demonstrated a novel method for room temperature fabrication of core−shell- and hollow-structured manganese carbonate/titania composites, utilizing a template-assisted protocol using $MnCO_3$ microspheres. TiO_2 coating on the $MnCO_3$ microsphere was achieved via two-step LPD process. The surface and internal morphologies of the particles are altered by the control of the prereaction time between MnCO3 and $[NH_4]_2TiF_6$ (first step), and the subsequent, conventional LPD reaction (second step) that results in the coating fixation. Protons generated as byproduct of the LPD reaction are used to remove the core at room temperature by simply controlling the reaction time. This exquisite combination of manganese carbonate and LPD reaction provides a new direction for the design of composite materials.

Calcination of the fabricated composite particles at an elevated temperature resulted in the simultaneous conversion of $MnCO_3$ remaining in the core and shell to α-Mn_2O_3 and of amorphous titania to anatase titania, with the preservation of the initial particle morphology. The fabricated core−shell and hollow particles showed very fast adsorption of methlylene blue along with high adsorption capacities, indicating that they can be potentially used in a wide range of applications using their morphological features, such as adsorbents of chemicals, photocatalysts, carriers or electrode materials. The proposed approach is simple and versatile, and thus can be utilized for green synthesis of several types of metal oxide composites with unique physical and chemical properties.

dx.doi.org/10.1021/am404052p | ACS Appl. Mater. Interfaces 2014, 6, 57−64

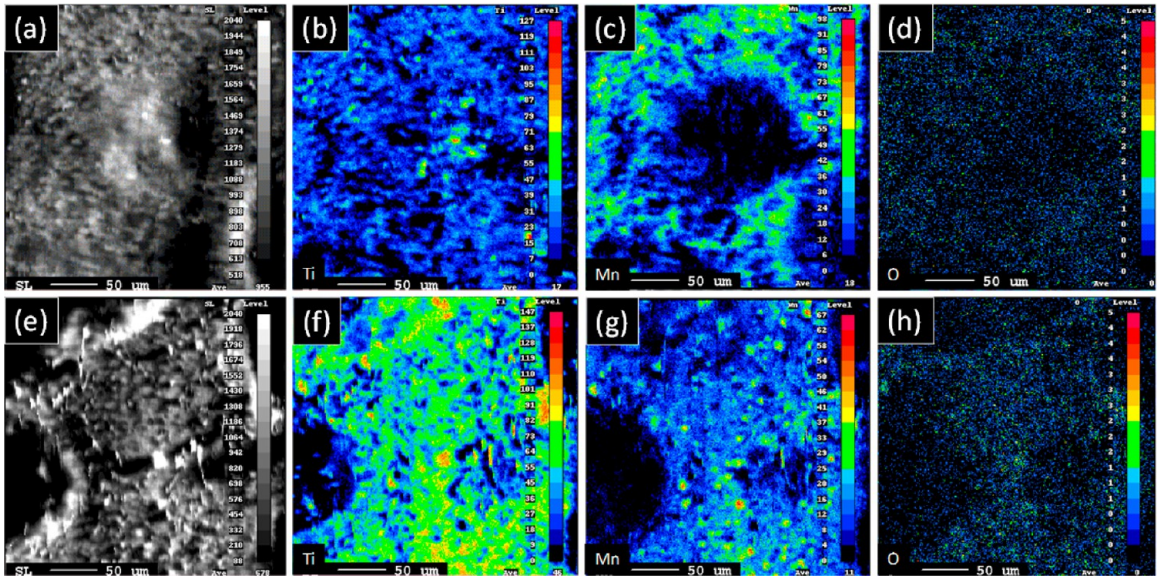

Figure 8. EPMA mapping images of Mn_2O_3/TiO_2 composites for Ti, Mn and O elements: (a–d) core–shell structure and (e–h) hollow structure.

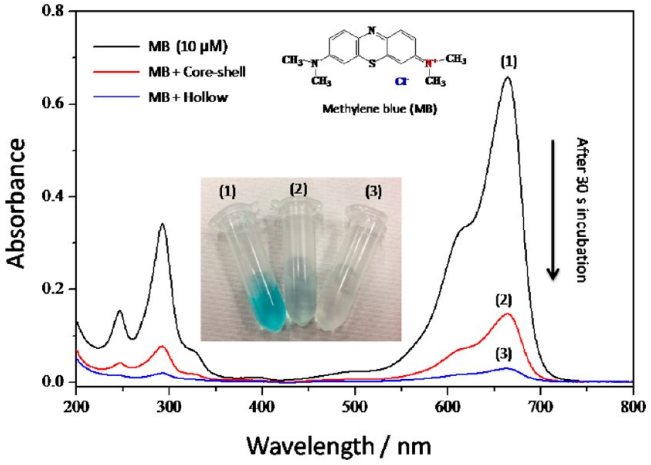

Figure 9. UV–vis absorption spectral changes of MB (10 μM in water) after 30 s incubation with Mn_2O_3/TiO_2 composites (1.5 g L^{-1}). Inset shows a photograph showing colorimetric image of MB (1) before and after adsorption test with (2) core–shell and (3) hollow composites.

■ ASSOCIATED CONTENT

Supporting Information

Additional results, including SEM images of products synthesized in different solvents; particle morphology dependence on reagent concentration and prereaction time; pH change during the reaction; SEM images of the composite products prepared with stratiform $MnCO_3$ templates; SEM images of core–shell $MnCO_3/TiO_2$ composite and core–shell Mn_2O_3/TiO_2 composite; final products color change dependent on the structure and EPMA results of Mn_2O_3/TiO_2 prepared by calcination. This material is available free of charge via the Internet at http://pubs.acs.org/.

■ AUTHOR INFORMATION

Corresponding Author

*Tel.: +81-93-695-3293. Fax: +81-93-695-3384. E-mail: leesw@kitakyu-u.ac.jp.

Author Contributions

H.K.L. performed the experiments with technical support from the coauthors and obtained data representation. S.W.L. supervised the whole work. The manuscript was written through contributions of all authors. All authors have given approval to the final version of the manuscript.

Notes

The authors declare no competing financial interest.

■ ACKNOWLEDGMENTS

This work was supported by MEXT via second Kitakyush Knowledge-based Cluster Project (Regional Innovation Cluster Program (Global Type). We sincerely thank Prof. Toyoki Kunitake for helpful discussions and Ms. Mari Tabaru for technical assistance during the BET measurements.

■ REFERENCES

(1) Feng, X.; Shankar, K.; Varghese, O. K.; Paulose, M.; Latempa, T. J.; Grimes, C. A. *Nano Lett.* **2008**, *8*, 3781–3786.
(2) Song, Y.-Y.; Schmidt-Stein, F.; Bauer, S. *J. Am. Chem. Soc.* **2009**, *131*, 4230–4232.
(3) Yu, J.-G.; Yu, H.-G.; Cheng, B.; Zhao, X.-J.; Yu, J. C.; Ho, W.-K. *J. Phys. Chem. B* **2003**, *107*, 13871–13879.
(4) Bischoff, B. L.; Anderson, M. A. *Chem. Mater.* **1995**, *7*, 1772–1778.
(5) Song, C.; Yu, W.; Zhao, B.; Zhang, H.; Tang, C.; Sun, K.; Wu, X.; Dong, L.; Chen, Y. *Catal. Commun.* **2009**, *10*, 650–654.
(6) Yang, G.; Hu, P.; Cao, Y.; Yuan, F.; Xu, R. *Nanoscale Res. Lett.* **2010**, *5*, 1437–1441.
(7) Pei, A.-H.; Shen, Z.-W.; Yang, G.-S. *Mater. Lett.* **2007**, *61*, 2757–2760.
(8) Xiong, Y.; Wiley, B.; Chen, J.; Li, Z.-Y.; Yin, Y.; Xia, Y. *Angew. Chem., Int. Ed.* **2005**, *44* (48), 7913–7917.
(9) Yang, H. G.; Zeng, H. C. *J. Phys. Chem. B* **2004**, *108*, 3492–3495.
(10) Tu, K. N.; Gösele, U. *Appl. Phys. Lett.* **2005**, *86*, art. no. 093111, pp. 1-3.
(11) Peng, Q.; Dong, Y.; Li, Y. *Angew. Chem., Int. Ed.* **2003**, *42*, 3027–3030.
(12) Zoldesi, C. I.; Imhof, A. *Adv. Mater.* **2005**, *17*, 924–928.
(13) Walsh, D.; Lebeau, B.; Mann, S. *Adv. Mater.* **1999**, *11*, 324–328.
(14) Caruso, F.; Caruso, R. A.; Möhwald, H. *Science* **1998**, *282*, 1111–1114.

(15) Yang, M.; Ma, J.; Zhang, C.; Yang, Z.; Lu, Y. *Angew. Chem., Int. Ed.* **2005**, *44*, 6727−6730.
(16) Arnal, P. M.; Weidenthaler, C.; Schüth, F. *Chem. Mater.* **2006**, *18*, 2733−2739.
(17) Kim, S.-W.; Kim, M.; Lee, W. Y.; Hyeon, T. *J. Am. Chem. Soc.* **2002**, *124*, 7642−7643.
(18) Zhang, N.; Xu, Y.-J. *Chem. Mater.* **2013**, *25*, 1979−1988.
(19) Zhang, N.; Liu, S.; Xu, Y.-J. *Nanoscale* **2012**, *4*, 2227−2238.
(20) Caruso, R. A.; Susha, A.; Caruso, F. *Chem. Mater.* **2001**, *13*, 400−409.
(21) Deki, S.; Aoi, Y.; Hiroi, O.; Kajinami, A. *Chem. Lett.* **1996**, *25*, 433−434.
(22) Deki, S.; Aoi, Y.; Asaoka, Y.; Kajinami, A.; Mizuhata, M. *J. Mater. Chem.* **1997**, *7*, 733−736.
(23) Deki, S.; Yoshida, N.; Hiroe, Y.; Akamatsu, K.; Mizuhata, M.; Kajinami, A. *Solid State Ionics* **2002**, *151*, 1−9.
(24) Ettireddy, P. R.; Ettireddy, N.; Mamedov, S.; Boolchand, P.; Smirniotis, P. G. *Appl. Catal. B Environ.* **2007**, *76*, 123−134.
(25) Tian, W.; Fan, X.; Yang, H.; Zhang, X. *J. Hazard. Mater.* **2010**, *177*, 887−891.
(26) Zhang, L.; He, D.; Jiang, P. *Catal. Commun.* **2009**, *10*, 1414−1416.
(27) Katagiri, K.; Ohno, K.; Masuda, Y.; Koumoto, K. *J. Ceram. Soc. Jpn.* **2007**, *115*, 831−834.
(28) Tong, W.; Gao, C. *Colloids Surf., A* **2007**, *295*, 233−238.
(29) Yamashita, T.; Vannice, A. *J. Catal.* **1996**, *161*, 254−262.
(30) Einaga, H.; Futamura, S. *J. Catal.* **2004**, *227*, 304−312.
(31) Seo, W. S.; Jo, H. H.; Lee, K.; Kim, B.; Oh, S. J.; Park, J. T. *Angew. Chem., Int. Ed.* **2004**, *43*, 1115−1117.
(32) Na, C. W.; Han, D. S.; Kim, D. S.; Park, J.; Jeon, Y. T.; Lee, G.; Jung, M. H. *Appl. Phys. Lett.* **2005**, *87*, 1−3.
(33) Thackeray, M. M.; Johnson, C. S.; Vaughey, J. T.; Li, N.; Hackney, S. A. *J. Mater. Chem.* **2005**, *15*, 2257−2267.
(34) Park, K. S.; Cho, M. H.; Park, S. H.; Nahm, K. S.; Sun, Y. K.; Lee, Y. S.; Yoshio, M. *Electrochim. Acta* **2002**, *47*, 2937−2942.
(35) Hu, C.-C.; Tsou, T.-W. *Electrochem. Commun.* **2002**, *4* (2), 105−109.
(36) Junhua, J.; Anthony, K. *Electrochim. Acta* **2002**, *47*, 2381−2386.
(37) Toupin, M.; Brousse, T.; Bélanger, D. *Chem. Mater.* **2004**, *16*, 3184−3190.
(38) Pourmortazavi, S. M.; Rahimi-Nasrabadi, M.; Davoudi-Dehaghani, A. A.; Javidan, A.; Zahedi, M. M.; Hajimirsadeghi, S. S. *Mater. Res. Bull.* **2012**, *47*, 1045−1050.
(39) Lei, S.; Peng, X.; Li, X.; Liang, Z.; Yang, Y.; Cheng, B.; Xiao, Y.; Zhou, L. *Mater. Chem. Phys.* **2011**, *125*, 405−410.
(40) Cao, J.; Zhu, Y.; Bao, K.; Shi, L.; Liu, S.; Qian, Y. *J. Phys. Chem. C* **2009**, *113*, 17755−17760.
(41) Antipov, A. A.; Shchukin, D.; Fedutik, Y.; Petrov, A. I.; Sukhorukov, G. B.; Möhwald, H. *Colloids Surf., A* **2003**, *224*, 175−183.
(42) King'Ondu, C. K.; Iyer, A.; Njagi, E. C.; Opembe, N.; Genuino, H.; Huang, H.; Ristau, R. A.; Suib, S. L. *J. Am. Chem. Soc.* **2011**, *133*, 4186−4189.
(43) Bilati, U.; Allémann, E.; Doelker, E. *Eur. J. Pharm. Sci.* **2005**, *24*, 67−75.